

A Study on the Speed Control of Induction Motor Using Modified SVPWM Control Method

Jae-Jung HUR[†]

Korea Institute of Maritime and Fisheries(professor)

변형된 SVPWM 제어기법을 이용한 유도전동기 속도제어에 관한 연구

허재정[†]

한국해양수산연수원(교수)

Abstract

This paper compares and analyzes the direct torque control method, which is widely used for induction motor speed control, and the indirect vector control method, which uses the modified SVPWM method, which has much lower computational power than the general SVPWM method. The modified SVPWM shows similar performance in the high speed range compared to the direct torque control method in speed, torque, input current, and load current control performance, but it shows remarkably superior performance in the low speed range. The computer simulations using the PISM program confirmed the characteristics of the control methods and verified their effectiveness.

Key words : Induction motor, Direct torque control, SVPWM, Speed control, torque

1. Introduction

Recently in the international maritime industry, various regulations have been tightened to reduce pollutants emitted from ships, especially the International Maritime Organization. To cope with this, various researches are being conducted to reduce air pollutants such as nitrogen oxides, sulfur oxides and carbon dioxide. s one of the solutions, researches are being actively conducted on the method of driving an electric motor using electricity generated from eco-friendly renewable energy such as a generator using LNG fuel, fuel

cell, solar energy and wind energy (Kim et al., 2009; Jeon et al., 2018; Kim et al.,2013).

Induction motors, which are highly applicable to small work boats and cruise ships used offshore, have a nonlinear multivariable control structure, which have been used mainly for constant speed applications because of their complicated speed control. However, with the development of power semiconductor technology, current control technology, control elements and control theory, it has the characteristics that are not inferior to the performance of DC motors in the driving field requiring high performance, It is relatively

[†] Corresponding author : 051-620-5789, jjheo@seaman.or.kr/orcid.org/0000-0002-0519-7717

inexpensive and robust compared to DC motors and is widely used in various power applications. In particular, vector control and direct torque control are applied to the fields that need instantaneous torque control or speed control. Induction motors are being expanded by using techniques that can control current and torque faster, such as hysteresis, triangular wave comparison, and space vector voltage modulation(Jeon et al., 2019).

For the propulsion induction motor, direct torque control methods that have the advantage of fast response and accuracy, control magnetic flux and torque independently, can change control precision and switching frequency by adjusting hysteresis band width using magnetic flux and torque error are used so many. However, the switching frequency is variable and there can be a lot of ripple in torque and speed and there is a disadvantage that the control characteristic is deteriorated when starting, the torque command changes and in the low speed region.

In this paper, it was confirmed that more stable motor control is possible by applying the indirect vector control method using the modified space vector modulation method to the existing propulsion induction motor which has been driven by the direct torque control method. Unlike the general space vector technique, the applied modulation method constructs the effective voltage in terms of the effective time applied and the space vector PWM can be implemented more simply while maintaining excellent existing performance. That is, the amount of calculation required for the triangular wave comparison current control technique is required, but excellent control performance similar to that of the existing SVPWM is exhibited(Kim et al., 2011; Yoon et al., 2009; Kim et al., 1995).

In small coastal ships, such as cruise ships and

small work vessels, where space constraints occur, AFE rectifiers(Hur et al., 2018; Jeon et al., 2017; Hareh and Ankit, 2016), which are a type of active filter instead of DFE rectifiers which require passive filters or phase shifting transformers to mitigate harmonics are installed, therefore, the modified SVPWM method is applied to the AFE rectifier and inverter to check the response characteristics when the load torque and speed command of the step input are applied to the induction motor, and then, the characteristics of the conventional direct torque control method and the modified SVPWM control method applied in this paper are compared and analyzed.

II . Materials and Methods

1. Space vector voltage modulation

Space vector voltage modulation is a technique of modulating the three-phase command voltage as a space vector in complex space.

<Table 1> Space vector according to switching state.

Switch status $S_a S_b S_c$	Phase voltage $v_{as} \quad v_{bs} \quad v_{cs}$			Space voltage vector V_n
0 0 0	0	0	0	$V_0 = 0 / 0^\circ$
1 0 0	$\frac{2}{3} V_{dc}$	$-\frac{1}{3} V_{dc}$	$-\frac{1}{3} V_{dc}$	$V_1 = \frac{2}{3} V_{dc} / 0^\circ$
1 1 0	$\frac{1}{3} V_{dc}$	$\frac{1}{3} V_{dc}$	$\frac{2}{3} V_{dc}$	$V_2 = \frac{2}{3} V_{dc} / 60^\circ$
0 1 0	$-\frac{1}{3} V_{dc}$	$\frac{2}{3} V_{dc}$	$-\frac{1}{3} V_{dc}$	$V_3 = \frac{2}{3} V_{dc} / 120^\circ$
0 1 1	$-\frac{2}{3} V_{dc}$	$\frac{1}{3} V_{dc}$	$\frac{1}{3} V_{dc}$	$V_4 = \frac{2}{3} V_{dc} / 180^\circ$
0 0 1	$-\frac{1}{3} V_{dc}$	$-\frac{1}{3} V_{dc}$	$\frac{2}{3} V_{dc}$	$V_5 = \frac{2}{3} V_{dc} / 240^\circ$
1 0 1	$\frac{1}{3} V_{dc}$	$-\frac{2}{3} V_{dc}$	$\frac{1}{3} V_{dc}$	$V_6 = \frac{2}{3} V_{dc} / 300^\circ$
1 1 1	0	0	0	$V_7 = 0 / 0^\circ$

This method can linearly generate a voltage that is 15.5% larger than the SPWM technique, and has the advantage that the harmonics in the current and torque are less than other techniques when the modulated voltage is applied to the motor. In this technique, since the command voltage is given as a space vector, the output voltage of the inverter needs to be expressed as a space voltage vector. As shown in [Fig. 1], a three-phase inverter has a total of eight different switching states: different three phase voltages. The space voltage vectors for three phase voltages corresponding to eight different switching states of these inverters are shown in <Table 1>.

Of these, six voltage vectors $V_1 \sim V_6$ are an active voltage vector for applying a valid voltage to a load, all of which are the same as $2V_{dc}/3$ and only different in phase. In contrast, the two voltage vectors V_0 and V_7 are called zero voltage vectors because they do not apply a valid voltage to the load. The use of this zero voltage vector has a great impact on the modulation performance.

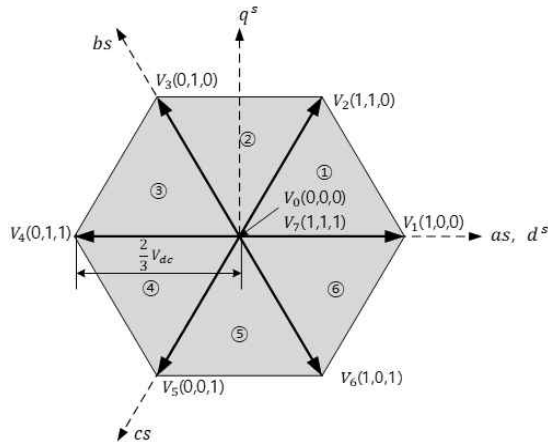


[Fig. 1] Space vector expressed in a complex number plane.

If the three-phase command phase voltage changes over time, the command voltage vector rotates counterclockwise in a complex space plane or d-q stationary coordinate system, as shown in [Fig. 2].

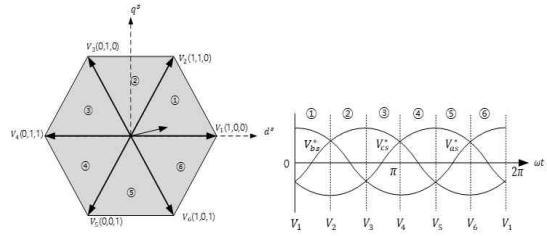


[Fig. 2] Movement of the reference voltage vector.

In the space vector modulation method, the command voltage given as the voltage vector is generated by using eight voltage vectors that can be generated by the inverter.

Two effective voltage vectors (V_n, V_{n+1}) adjacent to the reference voltage vector V^* and a zero voltage vector (V_0, V_7) are used to make an average voltage equal to the reference voltage vector for a predetermined modulation period.

That is, two effective voltage vectors V_1 and V_2 closest to the command voltage vector V^* among the effective voltage vectors are properly synthesized to form a voltage vector having the same magnitude and phase as the command voltage vector V^* . The process of synthesizing the voltage is generated in three stages, as shown in [Fig. 3], which is repeated for each voltage modulation period T_s determined by the switching frequency. First, it is assumed that the magnitude and phase of the command voltage vector V^* is constant during the modulation period. In the first step of synthesis, one vector V_1 of two effective voltage vectors adjacent to the command voltage vector V^*

is applied for T_1 and next, apply the remaining adjacent vector V_2 for T_2 to match the phase and magnitude with V^* . The same voltage as V^* can then be generated. Finally, if the sum of the application times T_1 and T_2 of the two vectors is less than the voltage modulation period T_s , the zero voltage vector V_0 or V_7 is applied for the remaining $T_0 (= T_s - T_1 - T_2)$ so that no further voltage is applied.

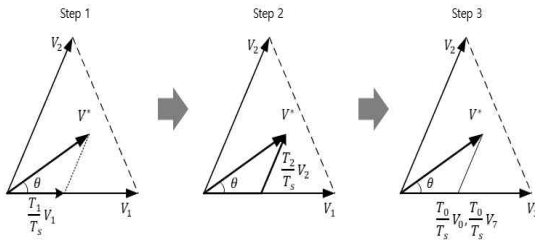


[Fig. 3] Process of voltage modulation.

The application times T_1 , T_2 and T_0 of two effective voltage vectors and zero voltage vectors required in this modulation process are shown in equation (1).

$$\int_0^{T_s} V^* dt = \int_0^{T_1} V_n dt + \int_{T_1}^{T_1+T_2} V_{n+1} dt \dots\dots\dots (1)$$

$$+ \int_{T_1+T_2}^{T_s} V_{0,7} dt$$

Assuming that the command voltage vector V^* and the direct current input voltage V_{dc} are constant during the voltage modulation period T_s , equation (2) is as follows.

$$V^* \cdot T_s = V_n \cdot T_1 + V_{n+1} \cdot T_2 \dots\dots\dots (2)$$

The formula of two complex axis components when the command voltage vector V^* is located in the region ① ($0 \leq \theta \leq 60^\circ$) is expressed as follows.

$$\begin{cases} T_s \cdot |V^*| \cdot \cos\theta = T_1 \cdot \left(\frac{2}{3} V_{dc}\right) \\ \qquad \qquad \qquad + T_2 \cdot \left(\frac{2}{3} V_{dc}\right) \cos 60^\circ \dots\dots (3) \\ T_s \cdot |V^*| \cdot \sin\theta = T_2 \cdot \left(\frac{2}{3} V_{dc}\right) \sin 60^\circ \end{cases}$$

In Eq. (3), $|V^*|$ and θ are the magnitude and phase of the voltage vector, respectively. The application times of the effective voltage vector and the zero voltage vector are calculated from this equation as follows.

$$T_1 = T_s \cdot a \cdot \frac{\sin(60^\circ - \theta)}{\sin 60^\circ} \dots\dots\dots (4)$$

$$T_2 = T_s \cdot a \cdot \frac{\sin \theta}{\sin 60^\circ} \dots\dots\dots (5)$$

$$T_0 = T_s - (T_1 + T_2) \dots\dots\dots (6)$$

here, $a = |V^*| / (\frac{2}{3} V_{dc})$

The application times of the effective voltage vector and the zero voltage vector in the remaining areas are also the same. In the space vector voltage modulation technique, the sum of the application times of the effective voltage vectors should not be greater than the modulation period T_s . That is, $T_1 + T_2 \leq T_s$. The magnitude of the command voltage that satisfies this condition can be obtained as shown in equation (7).

$$T_1 + T_2 \leq T_s \rightarrow V^* \leq \frac{V_{dc}}{\sqrt{3}} \frac{1}{\sin(60^\circ + \theta)} \dots\dots (7)$$

From Eq. (7), the range of modulated command voltage vectors is the inner region of the hexagon, which consists of six effective voltage vectors, as shown in [Fig. 4]. The maximum magnitude of the command voltage is $2V_{dc}/3$.

The inside of the circle inscribed in the hexagon in this area is the area of the command voltage capable of linear modulation. The radius of the

inscribed circle is $V_{dc}/\sqrt{3}$, which is the maximum value of fundamental phase voltage that can be output by the space vector voltage modulation technique, which is about 15.5% larger than the SPWM method. In addition, it corresponds to 90.7% of the voltage during 6-step operation.(Kim, 2016)

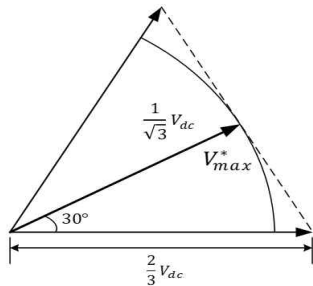


[Fig. 4] Controlled voltage areas in SVPWM.

A comparison of the voltage utilizations for the various PWM techniques is shown in <Table 2>.

<Table 2> Comparison of voltage utilization by modulation technique.

	Phase voltage (Fundamental wave max)	Square wave control criteria compare
Square wave control (6-step)	$\frac{2}{\pi} V_{dc}$	100 %
SPWM	$\frac{V_{dc}}{2}$	78.5 %
SVPWM	$\frac{V_{dc}}{\sqrt{3}}$	90.7 %

2. Modified Space Vector Modulation

Conventional space vector modulation is difficult to implement compared to other types of PWM because of the approach based on the position of the reference voltage vector in two-dimensional vector space. Since the calculation is performed based on the spatial region to which the reference

voltage vector belongs, the problem of double calculation that requires the calculation of the relationship with the actual voltage of the three phases to be output again is the biggest disadvantage of the existing SVPWM.

The modified SVPWM technique applied in this paper can implement SVPWM relatively simply while maintaining the existing performance by constructing SVPWM in terms of the valid time of applying the effective voltage. By the simple relocation algorithm of the newly developed zero-voltage vector, the applied PWM method shows the same performance as the existing SVPWM, furthermore it can be implemented more easily because the amount of calculation similar to the triangular wave comparison current control technique is required.

2.1 Space vector modulation pattern

In general SVPWM, voltage is treated as vector and analyzed in vector space. However, in real 3-phase inverter system, the time-base analysis can reduce the computational complexity because switching time determines three voltage states. Based on the d-q conversion theory, the reference phase voltage of an induction motor is as follows.

$$\begin{bmatrix} V_{as}^* \\ V_{bs}^* \\ V_{cs}^* \end{bmatrix} = \begin{bmatrix} 1 & 0 \\ -\frac{1}{2} & +\frac{\sqrt{3}}{2} \\ -\frac{1}{2} & -\frac{\sqrt{3}}{2} \end{bmatrix} \cdot \begin{bmatrix} V_d^{s*} \\ V_q^{s*} \end{bmatrix} \dots\dots\dots (8)$$

Using the reference phase voltage, switching time can be obtained directly from the basic concept of SVPWM without the hassle of checking and reassembling the region as in conventional SVPWM. To do this, check the relationship between the time T_1 , T_2 at which the effective vector is applied and the reference phase voltage.

Assuming the case where the reference voltage is located in the region ① ($0 \leq \theta \leq 60^\circ$) and $|V^*| \cdot \cos\theta$ is V_d^{s*} and $|V^*| \cdot \sin\theta$ is V_q^{s*} in equation (3), it can be expressed as follows.

$$\begin{cases} T_s \cdot V_d^{s*} = T_1 \cdot \left(\frac{2}{3} V_{dc}\right) \\ \quad + T_2 \cdot \left(\frac{2}{3} V_{dc}\right) \cos 60^\circ \dots\dots\dots (9) \\ T_s \cdot V_q^{s*} = T_2 \cdot \left(\frac{2}{3} V_{dc}\right) \sin 60^\circ \end{cases}$$

Equation (9) is expressed based on T_1 and T_2 as follows.

$$\begin{aligned} T_1 &= T_s \cdot \frac{3}{2V_{dc}} (V_d^{s*} - \frac{1}{\sqrt{3}} V_q^{s*}) \dots\dots\dots (10) \\ &= \frac{T_s}{V_{dc}} (\frac{3}{2} V_d^{s*} - \frac{\sqrt{3}}{2} V_q^{s*}) \\ &= \frac{T_s}{V_{dc}} (V_d^{s*} + \frac{1}{2} V_d^{s*} - \frac{\sqrt{3}}{2} V_q^{s*}) \\ &= \frac{T_s}{V_{dc}} (V_d^{s*}) + \frac{T_s}{V_{dc}} (\frac{1}{2} V_d^{s*} - \frac{\sqrt{3}}{2} V_q^{s*}) \\ &= \frac{T_s}{V_{dc}} (V_{as}^*) - \frac{T_s}{V_{dc}} (V_{bs}^*) = T_{as} - T_{bs} \end{aligned}$$

$$\begin{aligned} T_2 &= T_s \cdot \frac{3}{2V_{dc}} (\frac{2}{\sqrt{3}} V_q^{s*}) \dots\dots\dots (11) \\ &= \frac{T_s}{V_{dc}} (0 \cdot V_d^{s*} + \sqrt{3} V_q^{s*}) \\ &= \frac{T_s}{V_{dc}} (\frac{1}{2} V_d^{s*} + \frac{\sqrt{3}}{2} V_q^{s*} - \frac{1}{2} V_d^{s*} \\ &\quad + \frac{\sqrt{3}}{2} V_q^{s*}) \\ &= \frac{T_s}{V_{dc}} (\frac{1}{2} V_d^{s*} + \frac{\sqrt{3}}{2} V_q^{s*}) \\ &\quad - \frac{T_s}{V_{dc}} (\frac{1}{2} V_d^{s*} - \frac{\sqrt{3}}{2} V_q^{s*}) \\ &= \frac{T_s}{V_{dc}} (V_{bs}^*) - \frac{T_s}{V_{dc}} (V_{cs}^*) = T_{bs} - T_{cs} \end{aligned}$$

From the equations (10), (11), the time difference at which the switching state change of each phase voltage of the induction motor is represented by the effective vectors T_1 and T_2 . In

the other five regions, we can obtain relations similar to equations (10), (11). At this time, the time T_{as} , T_{bs} , T_{cs} at which the phase voltage transitions is a ratio between the reference phase voltage and the DC voltage for a predetermined period as shown in equation (12).

$$\begin{aligned} T_{as} &= T_s \cdot \frac{V_{as}^*}{V_{dc}}, \\ T_{bs} &= T_s \cdot \frac{V_{bs}^*}{V_{dc}}, \dots\dots\dots (12) \\ T_{cs} &= T_s \cdot \frac{V_{cs}^*}{V_{dc}} \end{aligned}$$

With the proviso that $V_{as}^* + V_{bs}^* + V_{cs}^* = 0$ is $T_{as} + T_{bs} + T_{cs} = 0$.

The time when the effective vector is applied in the SVPWM is actually the time of applying the line voltage as the difference of each phase voltage of the induction motor. Assuming that each phase voltage transitions from V_{dc} to 0 [V] within one period, when the reference voltage is given to the region① as shown in the above formulas, we can see that the voltage as shown in [Fig. 5](a) is applied to the induction motor. In other words, a DC link voltage is applied between the a-b lines during T_1 , between the b-c lines during T_2 , and between the a-c lines during $T_1 + T_2$. Thus, the valid time T_1 , T_2 in the conventional SVPWM can be defined as the time difference between the time when the switching state of each phase of the induction motor transition. After calculating each region separately in the existing SVPWM, these times must be recalculated to the actual switching times, which requires a lot of computation time and inefficient efficiency. If SVPWM is analyzed in terms of the effective time that zero voltage is

applied to each line voltage rather than the idea that SVPWM is a space vector, it can be found that the times required to apply voltage on each phase of the induction motor are automatically calculated without distinguishing between sectors. When the reference phase voltages V_{as}^* , V_{bs}^* and V_{cs}^* are obtained from the reference voltages given to the vector, and the time periods T_{as} , T_{bs} and T_{cs} are applied to the phase voltages are calculated, the times when the phase voltages are applied already include the information on the voltages applied to the line voltages. This means that there is no need to recombine the effective time for each region or to know the reference phase voltage position in the vector space.

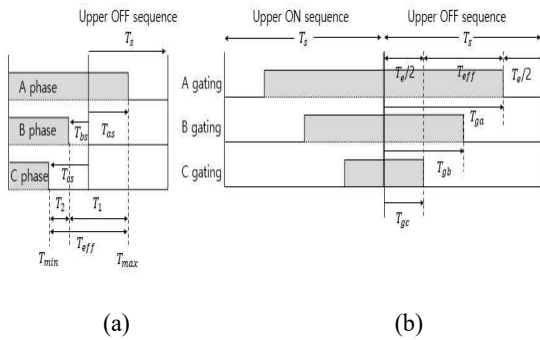


[Fig. 5] Switching pattern generation method of the applied SVPWM.

Of course, T_{as} , T_{bs} and T_{cs} times are virtual points at which the voltage applied to each phase is changed from 0 to V_{dc} or V_{dc} to 0. Only the difference in each time has a physical meaning. These are referred to as virtual switching times as variables for obtaining the actual switching time. [Fig. 5] is a conceptual diagram of the modified SVPWM. [Fig. 5](a) shows the virtual switching time that produces the calculated phase voltage of the induction motor when the reference

phase voltage is located in the region①. Since the neutral point potential of the induction motor is not fixed, from the recognition that the line voltage of the induction motor is the only valid voltage, by adding an arbitrary delay time to the virtual switching time in which the (-) time value exists, the actual switching time for the inverter can be selected without any difference. That is, if all switching operations are completed in one period, the general switching pattern as shown in [Fig. 5](b) can be obtained by shifting the valid time portion of [Fig. 5](a). The effective time T_{eff} in [Fig. 5](a) is the voltage between T_{max} and T_{min} . There is a way to move T_{eff} to any part of the period, but as T_{eff} is centered, as shown in [Fig. 5](b), the ripple of the current can be minimized. First, the actual switching time is obtained as shown in equation (13) by adding a specific deviation to the virtual switching time.

$$\begin{aligned}
 T_{ga} &= T_{as} + T_{offset} \\
 T_{gb} &= T_{bs} + T_{offset} \dots\dots\dots (13) \\
 T_{gc} &= T_{cs} + T_{offset}
 \end{aligned}$$

Equation(14) can be obtained from the fact that T_{eff} should be located at the center of one sampling period.

$$\begin{aligned}
 T_{eff} &= T_{max} - T_{min} \\
 T_{zero} &= T_s - T_{eff} \\
 T_{min} + T_{offset} &= T_{zero}/2 \dots\dots\dots (14) \\
 T_{offset} &= T_{zero}/2 - T_{min}
 \end{aligned}$$

Among the virtual switching points T_{as} , T_{bs} and T_{cs} the largest and smallest values are T_{max} and T_{min} . Therefore, three virtual switching points

should be arranged by time. Since what has been described so far is related to the case where the switching signal is OFF, the case of ON should also be considered. However, since the switching pattern is symmetric every two periods of sampling, using the fact that the voltage applied to the induction motor does not change no matter where the T_{eff} is placed, you can generate the pattern simply when the switching signal is turned on as in equation(15).

$$\begin{aligned}
 T_{ga}(ON) &= T_s - T_{ga}(OFF) \\
 T_{gb}(ON) &= T_s - T_{gb}(OFF) \dots\dots\dots (15) \\
 T_{gc}(ON) &= T_s - T_{gc}(OFF)
 \end{aligned}$$

This can be obtained simply by adding the switching time in which the switch is turned ON to the switching time at the switch OFF.

Using the concept of the effective time (T_{eff}), SVPWM can be easily implemented in the phase voltage formula of the reference voltage. Unlike the conventional SVPWM, there is no need to check the region where the reference voltage vector is located, to select the applied vector, or to calculate the valid application time and recombine it. SVPWM can be easily implemented by simply moving the calculated virtual point in time using a simple three-element sorting algorithm. Therefore, the modified SVPWM method, which is applied to this paper, is very simple to implement in the low cost controller with low performance because the computational structure is very simple and the computation time is shorter than that of general SVPWM.

The switching pattern of SVPWM applied in this paper is shown in [Fig. 6]. After the valid time is obtained from the reference phase voltage, the actual switching time is obtained by shifting the

valid time over time. If the switch is changed to the ON state, it is moved symmetrically based on time 0.

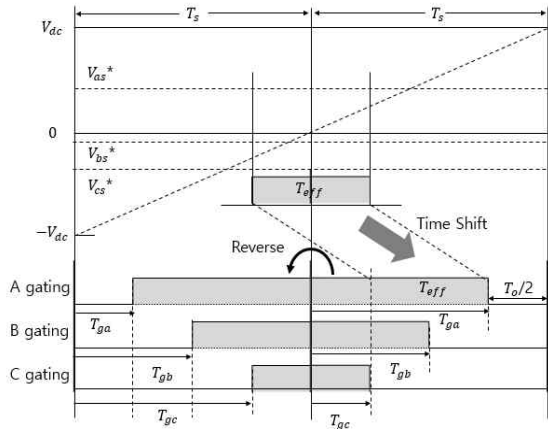


[Fig. 6] Implementation of the PWM method.

<Table 3> shows the difference in computation between general SVPWM and applied SVPWM. Compared to the complicated method of implementing conventional SVPWM, the amount of computation is greatly reduced, so it can be seen that SVPWM can be simply implemented(Kim and Sul, 1995)

<Table 3> Comparison of the calculation burden between the Conventional SVPWM and the Modified SVPWM

Operation type	Conventional SVPWM	Modified SVPWM
Comparative calculation (quarter)	4	5
Multiplication(x)	16	7
Division(÷)	1	1
Add-Subtraction(+,-)	15	11
Allocation calculation(=)	16	20
Logic calculation(xor)	1	1

III. Results and Discussion

1. Simulation

In order to prove the effectiveness of the modified SVPWM technique for the induction motor speed control algorithm, computer simulations were performed using the PSIM program in the high and low speed regions.

In the low speed region(300[rpm]), step load torque was applied and in the high speed region(1500[rpm]), the load was proportional to the speed square.

<Table 4> shows the parameters and system constants of the induction motor used in the simulation.

[Fig. 7] shows the PSIM block diagram of induction motor driving simulation.

<Table 4> Parameters of induction motor and system constants used for computer simulation.

Rated output	3[HP]	R_r	1.56 [Ω]
Rated voltage	220[V]	L_s	180[mH]
Rated current	9[A]	L_r	180[mH]
Rated speed	1735[rpm]	L_m	176[mH]
		J	
Poles	4	(Moment of inertia)	0.1[Kg·m ²]
R_s	2.0 [Ω]	Sampling cycle	100 [μ s]

1.1 Induction motor high speed range

[Fig. 8] & [Fig. 9] shows the speed response characteristics of the induction motor when the speed command is applied from 0 [rpm] to 1,500 [rpm].

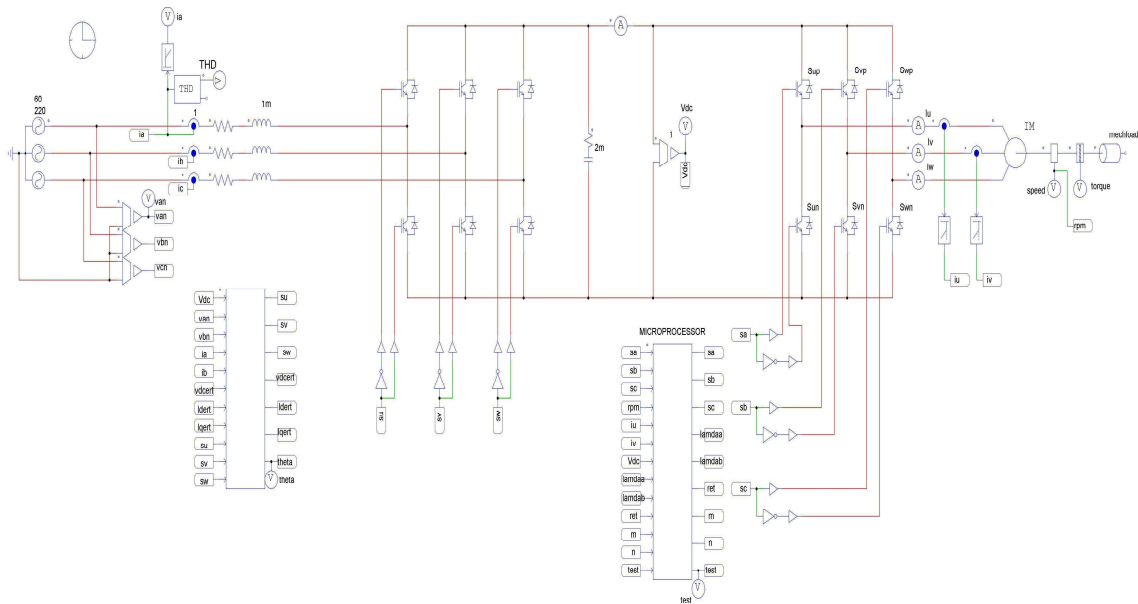
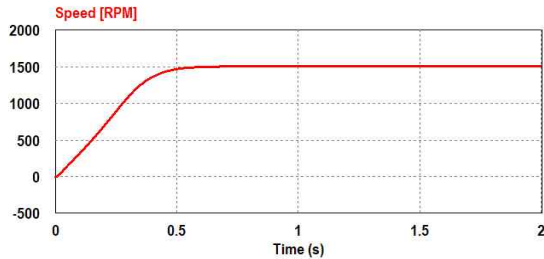
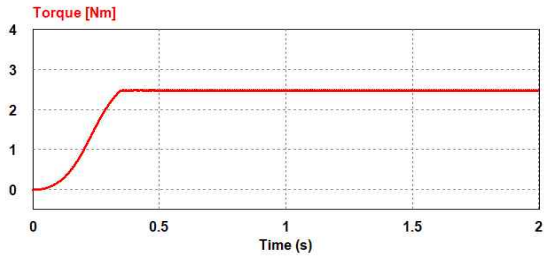


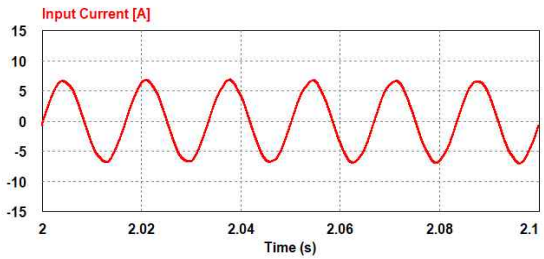
[Fig. 7] PSIM diagram of induction motor driver.



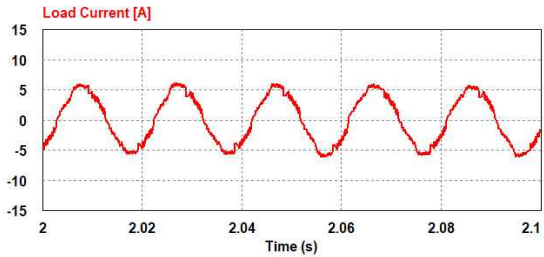
(a) Speed



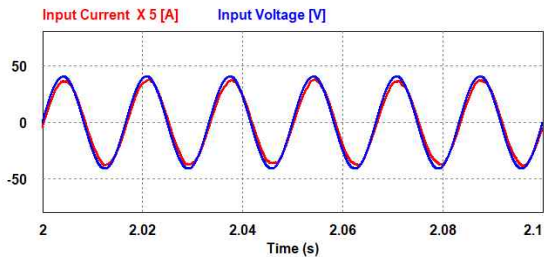
(b) Torque



(c) Input current

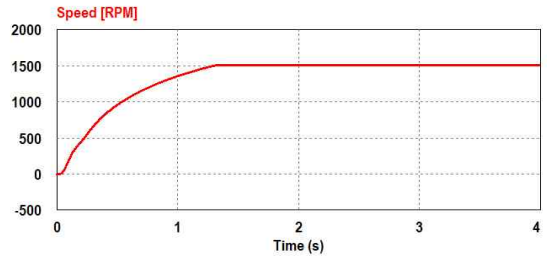


(d) Load current

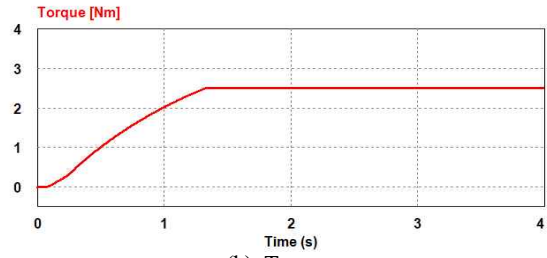


(e) Phase voltage and current

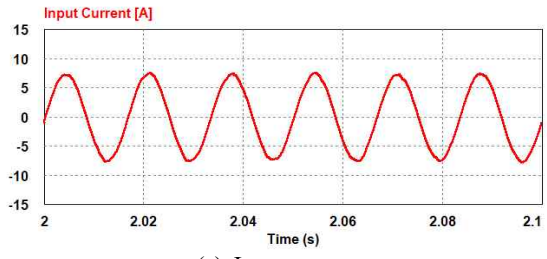
[Fig. 8] Simulation responses for step change of speed setting of DTC control(0→1,500[rpm]).



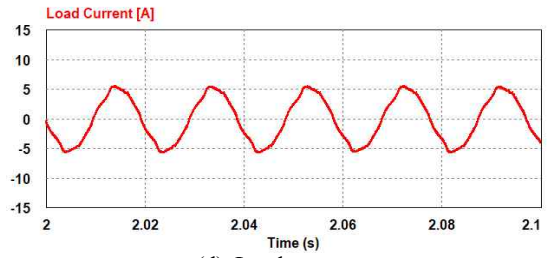
(a) Speed



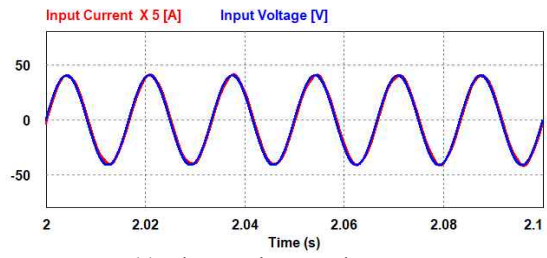
(b) Torque



(c) Input current



(d) Load current

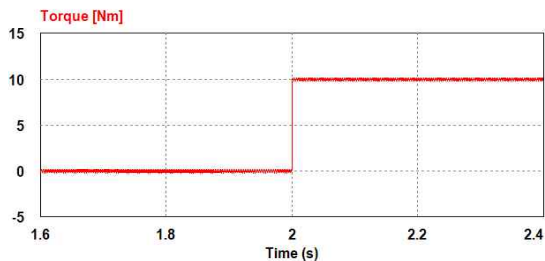
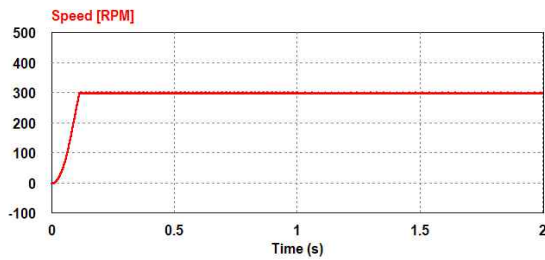


(e) Phase voltage and current

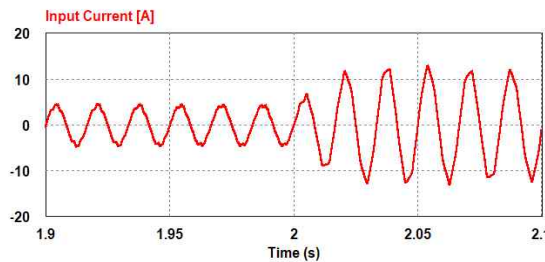
[Fig. 9] Simulation responses for step change of speed setting of modified SVPWM control(0→1,500[rpm]).

1.2 Induction motor low speed range

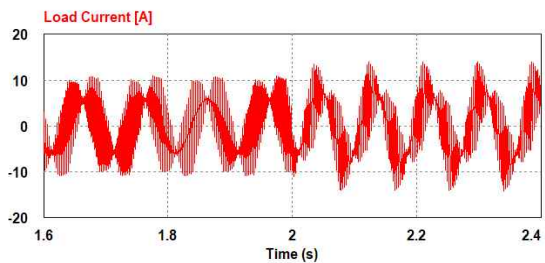
[Fig. 10] & [Fig. 11] shows the response state when load torque of 10 [N·m] is applied during steady state operation at 300 [rpm].



(b) Torque

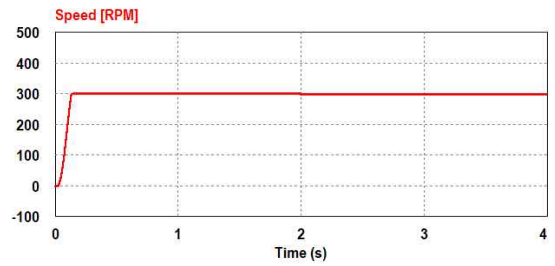


(c) Input current

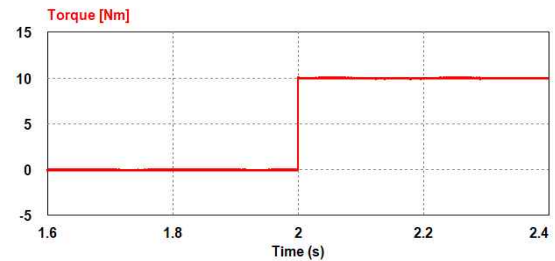


(d) Load current

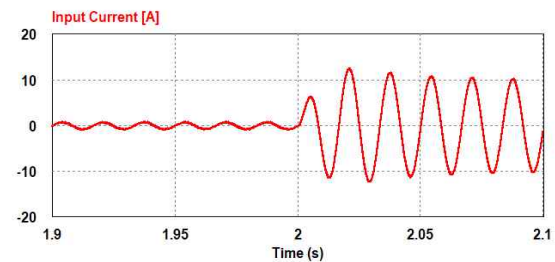
[Fig. 10] Simulation responses for step change of load torque of DTC control(300[rpm], 10[N·m]).



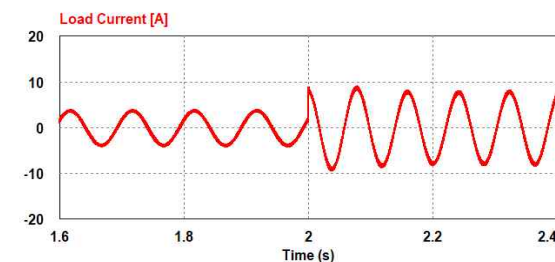
(a) Speed



(b) Torque



(c) Input current



(d) Load current

[Fig. 11] Simulation responses for step change of load torque of modified SVPWM control(300[rpm], 10[N·m]).

2. Review simulation results

When comparing [Fig. 8](a) and [Fig. 9](a), [Fig.

8](b) and [Fig. 9](b), the direct torque control method and the modified SVPWM technique are applied when the speed command is applied from 0[rpm] to 1,500[rpm], which is the high speed range. They were found that the speed and torque are stably controlled.

When comparing [Fig. 8](c) and [Fig. 9](c), the THD included in the input stage current is 3.41[%] in the direct torque control method and 2.71[%] in the modified SVPWM method, showing a current waveform close to the sine wave. It has been confirmed that the input current is very good quality.

When comparing [Fig. 8](d) and [Fig. 9](d), the maximum value of the load current is not much different between 4.6[A] and 4.7[A] in the steady state section, respectively in two methods. It can be seen that the current is controlled stably in the transient period.

When comparing [Fig. 10](a) and [Fig. 11](a), [Fig. 10](b) and [Fig. 11](b), when the speed command is applied from 0[rpm] to 300[rpm], which is a low speed range, in the direct torque control method it is confirmed that the fine oscillation of speed and torque occurs in the steady state section, and in the modified SVPWM method, the speed and torque are stably controlled.

When comparing [Fig. 10](c) and [Fig. 11](c), THD of 5.32[%] included in the input torque of direct torque control method is shown in the steady state section where load is applied. The input current waveform of the modified SVPWM is 3.34[%], which shows that the input current of better quality is supplied and the change of current is faster according to the load variation.

In comparison between [Fig. 10](d) and [Fig. 11](d), the maximum load current values of the direct torque control method and the modified

SVPWM method are 6.8 ~ 12.8[A] and 9.1[A] in the steady state section after applying the load torque, respectively. It was found that the modified SVPWM method was controlled very stably, and it was confirmed that the SVPWM method was able to control stably even when the load was applied, even between the tools.

In comparison between [Fig. 8](e) and [Fig. 9](e), both of two methods, the power factor is 0.99, which is very good as the AFE rectifier is applied.

IV. Conclusion

In order to verify the performance of speed control of induction motors that can be used for propulsion in small electric propulsion ships, computer simulations using PSIM programs were conducted.

1. The SVPWM method applied in this paper shows similar or superior performance to the conventional direct torque control method in the high speed range.
2. Compared to the direct torque control where oscillation occurs at speed and torque load current in the low speed range, the control is more stable in SVPWM method.
3. It was confirmed that the current performance during load fluctuation is faster in the modified SVPWM method.

It is expected that the modified SVPWM method will help to improve the steering performance in small offshore electric propulsion ships where speed is slow and speeded up & down by frequent entry and exit ports.

References

- Hareesh P and Ankit S(2016). A novel control method for UPS battery charging using Active front End(AFE) PWM rectifier, IEEE power electronics, Drives and Energy System, Trivandrum, India, December 14~17, 978~980.
<https://doi.org/10.1109/PEDES.2016.7914232>
- Hur JJ, Kang KW, Kim JS and Kim SH(2018). Speed control for direct current motor using an AFE rectifier, Journal of the Korean Society of Marine Engineering, 42(10), 892~836.
<https://doi.org/10.5916/jkosme.2018.42.10.829>
- Jeon CH, Hur JJ, Yoon KK, Yoo HH and Kim SH(2019). Current control for an AFE Rectifier Using Space Vector PWM, Journal of the Korean Society of Marine Environment & Safety, 25(4), 498~503. [Online]. Available:
<https://doi.org/10.7837/kosomes.2019.25.4.498>
- Jeon HM, Kim SW and Kim JS(2018). A Study on Application of Electric Propulsion System using AFE Rectifier for Amall Coastal Vessles, Journal of the Korean Society of Marine Environment & Safety, 24(3), 373~380.
<https://doi.org/10.7837/kosomes.2018.24.3.373>
- Jeon HM, Yoon KK and Kim JS(2017). A study to Improve the DC output Waveforms of AFE Three-Phase PWM Rectifiers, Journal of the Korean Society of Marine Environment & Safety, 23(6), 739~745.
<https://doi.org/10.7837/kosomes.2017.23.6.739>
- Kim SH(2016). Motor control - DC, AC, BLDC. 2nd Edition. Bukdu PRESS. 114~140
- Kim JS and Sul SK(1995). A Novel Voltage Modulation Technique of the Space Vector PWM, The Korean Institute of Electrical Engineers, 44(7), 866~874.
- Kim JS, Oh SG and Kim SH(2009). A Study on the Speed and Torque Control of Propulsion Motor for Electric Propulsion Ship by Direct Torque Control, Journal of the Korean Society of Marine Engineering, 33(6), 946~951.
- Kim JS, Seo SD and Kim SH(2011). A Study on the Sensorless Speed Control of Induction Motor by New Direct Torque Control, Journal of the Korean Society of Marine Engineering, 35(8), 1105~1110,
<http://dx.doi.org/10.5916/jkosme.2011.35.8.1105>
- Kim SY, Cho BG, and Sul SK(2013). Consideration of active - front-end rectifier for electric propulsion navy ship., IEEE Energy Conversion Congress and Exposition, Denver, USA CO, 13~19.
<https://doi.org/10.1109/ECCE.2013.6646675>
- Yoon KK, Oh SG, Kim JS, Kim YS, S. Lee SG and Kim SH(2009). A Study on the Sensorless Speed Control of Induction Motor using Direct Torque Control, Journal of the Korean Society of Marine Engineering, 33(8), 1261~1267.

-
- Received : 05 February, 2020
 - Revised : 06 April, 2020
 - Accepted : 10 April, 2020